

# A Temporal Analysis Indicates a Mildly Relativistic Compact Jet in GRS 1915+105

Brian Punsly<sup>1</sup>

and

Jérôme Rodriguez<sup>2</sup>

## ABSTRACT

Most of our knowledge of the radio morphology and kinematics of X-ray binary partially synchrotron self-absorbed compact jets (hereafter compact jets) is based on the observations of GRS 1915+105 which has the most prominent compact jet. Yet, the compact jet bulk velocity,  $v$ , is poorly constrained in the literature,  $0.07 < v/c < 0.98$ . In spite of this uncertainty, compact jets are often unified with relativistic jets in active galactic nuclei. We have estimated  $v$  as part of a temporal analysis of GRS 1915+105 jets in “high plateau states” (HPS). We define the HPS as a state showing a hard X-ray spectrum and low level of long-term ( $> 10$ s) X-ray activity associated with 15 GHz flux density  $> 70$  mJy for  $> 7$  consecutive days. The radio emission is associated with compact jet emission. Two HPS were monitored at 15 GHz during their termination with e-folding times of 3.8 hrs and 8.6 hrs. We combine this time scale with the scale of spatial variation of the linear source of a VLBA image preceding the fade of one of these HPS in order to estimate the jet speed. Our assumption that the reduction in radio emissivity propagates as an approximate discontinuity down the HPS jet (leaving a weak jet in its wake) indicates  $0.17 < v/c < 0.43$ . This agrees closely with the only other existing  $v$  estimates that are derived directly from radio images, jet asymmetry produced by Doppler enhancement.

*Subject headings:* Black hole physics — X-rays: binaries — accretion, accretion disks

---

<sup>1</sup>1415 Granvia Altamira, Palos Verdes Estates CA, USA 90274 and ICRANet, Piazza della Repubblica 10 Pescara 65100, Italy, brian.punsly1@verizon.net

<sup>2</sup>Laboratoire AIM, CEA/DRF-CNRS-Université Paris Diderot, IRFU SAp, F-91191 Gif-sur-Yvette, France.

## 1. Introduction

Galactic black hole X-ray binaries (BHXRb) appear as compact flat spectrum radio sources during X-ray hard states (Corbel et al. (2000, 2003); Gallo et al. (2003)), that is widely interpreted as partially synchrotron self-absorbed compact jets (hereafter compact jets; e.g. Kaiser (2006)). The “compact jet” is suppressed during transition to the soft X-ray states (Fender et al. 1999b). GRS 1915+105 has the most prominent compact jet, an order of magnitude more luminous than that of other BHXRb. Thus, it is the only compact jet with a rich history of VLBI observations (Dhawan et al. 2000; Fuchs et al. 2003; Ribo et al. 2004). As opposed to conical SSA jets, the properties of GRS 1915+105 are better explained with a structured jet (see e.g. Punsly (2011)). The X-ray luminosity of GRS 1915+105 is also one of the highest of any known Galactic black hole candidate (Done et al. 2004). The existence of both a jet and high continuum luminosity make it tempting to speculate that GRS 1915+105 might be a scaled down version of a radio-loud quasar. This speculation has been further fueled by the highly publicized relativistic discrete ejections (Mirabel and Rodriguez 1994; Fender et al. 1999a).

The compact jet is one of three distinct radio phenomenon associated with GRS 1915+105. In this article, we emphasize the distinct character of these radio states. Much clarity has been attained in the classification of radio states by considering the X-ray evidence associated with each type of radio emission.

1. Major superluminal, discrete ejections are preceded by a hard X-ray flare that begins a few hours before jet launching. The strength of the X-ray flare is correlated with the kinetic luminosity of the ejection and are a sizeable fraction of the Eddington luminosity for powerful flares. During the jet launching, the X-ray flux is highly variable with a time average value roughly equal to the pre-flare level (Punsly and Rodriguez 2013a).
2. The continuous compact jet is accompanied by a hard X-ray state that is steady. Using the classifications of Belloni et al. (2000), a  $\chi$  class of X-ray variability state coexists with the compact jet (Klein-Wolt et al. 2002)
3. Quasi-periodic radio states are associated with oscillations of the X-ray light curves that are near their nadir when the ejection occurs. These are highly variable X-ray luminosity classes, showing fast transitions between hard and soft, very intense states. These states oscillate between low/hard and high/soft with the transition between low/hard and high/soft marked by an X-ray spike, that is the moment of the discrete radio ejection. These radio oscillations typically have peaks of 10 mJy - 50 mJy in the radio (Klein-Wolt et al. 2002; Rodriguez et al. 2008; Pooley and Fender 1997). It was shown in Rodriguez et al. (2008) that a bright soft spike preceded each ejection

similar to the discrete ejections described in (1). It should be noted that these quasi-periodic events include weak optically thin bubbles of radio emission (a few mJy), Rodriguez et al. (2008), and more powerful optically thick oscillations (Mirabel et al. 1998; Dhawan et al. 2000).

The luminous compact jets, being more ubiquitous than luminous relativistic discrete ejections in GRS 1915+105, have received most of the observational attention. Yet, the compact jet has no direct measurement of jet bulk velocity. This has led to some indirect estimates of bulk velocity. The primary motivation of our temporal analysis is to provide an independent determination of the compact jet bulk velocity derived directly from observation. As a corollary to this effort, we attempt to bring clarity to the notion of the continuous steady compact jet. A major source of confusion occurs in the interpretation of the compact jet as a consequence of radio imagery. Due to the insufficient u-v coverage and sensitivity of VLBA (Very Large Baseline Array) observations, the jet during highly variable (quasi-periodic) modest radio luminosity states ( $\sim 15\text{--}50$  mJy at 15 GHz) appears to have the same morphology as the jet in strong “steady” states ( $\sim 100\text{--}150$  mJy at 15 GHz), a twin exhaust flame (Dhawan et al. 2000). Thus, the compact nature of the jets in steady states and during quasi-periodic radio states are often considered without distinction (Dhawan et al. 2000). It is tempting to combine superluminal discrete ejections, the steady continuous compact jet and the stronger quasi-periodic radio states in a unified scheme based on the observational evidence for a common jet direction in all three cases (Dhawan et al. 2000). However, the degree to which these phenomena can be consolidated into one jet model is a subject of conjecture and is yet to be established by direct observational measurement (Fender et al. 2004). The compact jet is consistent with continuous radio emission on time scales as short as tens of seconds and for this reason it is distinct from the phenomenon that creates the quasi-periodic radio oscillations (see Section 4). The quasi-periodic radio emission is often assumed to arise from discrete ejecta, but emission cycles might also be a consequence of shocks or dissipative MHD wave trains within a jet (Dhawan et al. 2004). The desire to combine the three radio phenomenon in a unified model has led to speculation about the compact jet bulk velocity. It has been argued that since superluminal ejecta often appear before or after a compact jet that the compact jet must also be relativistic (Dhawan et al. 2000). But, this has never been directly observed and is still a conjecture (Ribo et al. 2004). The case was further bolstered by the idea that quasi-periodic ejecta would have to expand at near the speed of light if adiabatic cooling is the source of the fading of the ejecta (Dhawan et al. 2000). However, this argument is not direct because (as we show in Section 4) the continuous compact jet shows no quasi-periodic behavior in the radio (Klein-Wolt et al. 2002). Thusly motivated, the main goal of this paper is to add an independent method of determining the compact jet bulk velocity directly from observation to our knowledge base.

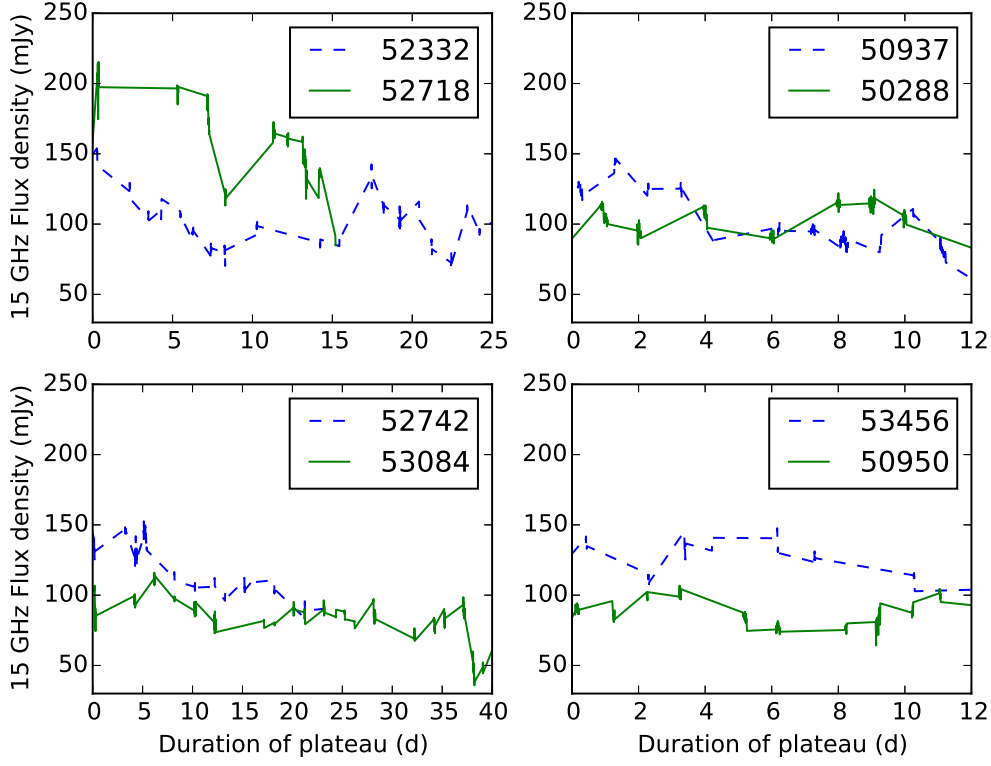


Fig. 1.— The 15 GHz light curves of the 8 high plateau states studied in this article. These states are very stable for GRS 1915+105, having modest to small variations on time scales of hours to a day.

Table 1: High Plateau States

Start Date (MJD)	Duration (Days)	Maximum 15 GHz Flux Density <sup>a</sup>	Minimum 15 GHz Flux Density <sup>a</sup>
50288	9	118 mJy	93 mJy
50937	11	121 mJy	87 mJy
50950	12	105 mJy	79 mJy
52332	28	139 mJy	73 mJy
52718	15	209 mJy	75 mJy
52742	25	144 mJy	89 mJy
53084	37	111 mJy	71 mJy
53456	10	141 mJy	109 mJy

<sup>a</sup>Flux density averaged over duration of the Ryle telescope observation on that day

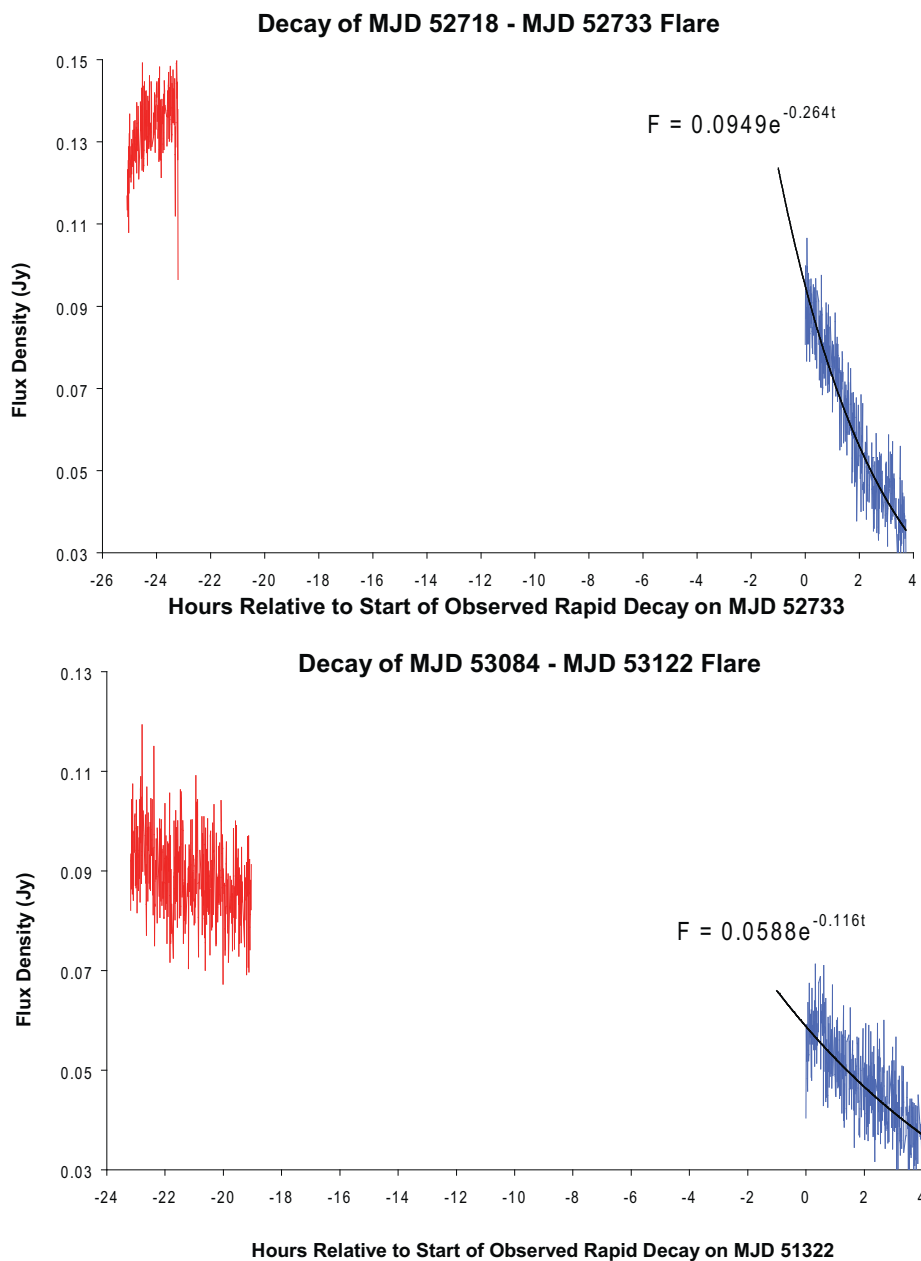


Fig. 2.— The Ryle Telescope was used to produce light curves of the decay of two of the HPS. The 15 GHz flux density,  $F$ , is fit by an exponential function during the decay. The unit of time in the exponential fit is hours. The decay on MJD 52733 in the top frame and on MJD 53122 in the bottom frame have e-folding times of 3.8 hrs and 8.6 hrs, respectively.

In this study, we search for some evidence in the radio data that could provide an indication of the bulk velocity of the compact jet in GRS 1915+105. Our method considers “high plateau states” (HPS, hereafter) that are defined by more than 70 mJy of flux density at 15 GHz for more than 7 days of monitoring. These radio states are always accompanied by an X-ray  $\chi$  state. The high plateau states are by all accounts strong compact jets and they provide an excellent background on which to study temporal variations of a stable structure. The large flux density allows short 32 s sampling with reasonably good statistics. There are 8 such high plateau states in the Ryle Telescope 15 GHz archive (Rushton et al. 2010). These 8 states are defined in Table 1. The light curves are shown in Figure 1.

In section 2, the bulk compact jet velocity is estimated. By comparing the time constant,  $T$ , of the exponential decay of the 15 GHz light curve that terminates two HPS with the spatial exponential decay constant,  $D$ , for the linear source of the VLBA imaged compact jets in HPS, we estimate the jet velocity,  $V = D/T$ . In Section 3, we compare and contrast the X-ray properties during the HPS and during the exponential decay of the radio light curve. A time series analysis of the radio data during HPS is presented in Section 4. These findings are summarized and consolidated into the unified scheme in the Discussion.

## 2. Bulk Velocity Estimate

In this section, we estimate the jet bulk velocity. Our method combines the timescale for the exponential decay of radio emission at the end of the HPS state with the characteristic spatial extent of a HPS jet, as determined in Sect. 2.3. Figure 1 shows the long term 15 GHz light curves of the eight HPS that have been monitored with the Ryle telescope (Rushton et al. 2010). There are gaps in the daily coverage in Figure 1, so the length of each HPS in Table 1 might be slightly under estimated in some cases. On days when the data was taken, the source was sampled continuously by the Ryle telescope for 30 minutes to 8 hours. Note that the strong HPS that begins on MJD 52718 is terminated by a decay then a major ejection before another HPS starts on MJD 52742 and the two events are formally two separate HPS (Fuchs et al. 2004).

Figure 2 shows the serendipitous capture of the decay of two of the eight HPS in Figure 1. The light curves are well fit by an an exponential decay. The decay on MJD 52733 in the top frame and on MJD 53122 in the bottom frame have e-folding times of 3.8 hrs and 8.6 hrs, respectively.

In order to determine a bulk flow speed from these decay times, one needs a measure of the propagation distance along the jet relative to the core. It is proposed that a relevant

distance can be attained by an analysis of the VLBA images of jet at the same frequency as the light curves in Figure 2, 15 GHz. The decline in flux indicates that the engine feeding the jet has either turned off or has been reduced significantly in strength. After this occurs, one expects that a discontinuity propagates along the jet leaving a weak jet in its wake. The previously ejected synchrotron emitting plasma continues to move along the conduit formed by the steady state HPS jet. There is no apriori reason for the geometry of the outflow of the previously ejected synchrotron emitting plasma to be altered from its steady state HPS configuration to zeroth order. Thus, one should be able to combine the e-folding distance for spatial decay of the empirically determined source of the VLBA image,  $D$ , with the e-folding decay times,  $T$  in Figure 2 to yield an apparent bulk flow jet velocity,  $V_{app} = D/T$ . This can be transformed to a physical bulk velocity,  $v$ , by the transformation

$$V_{app} = \frac{(v/c) \sin \theta}{1 - (v/c) \cos \theta} , \quad (1)$$

where  $\theta = 60^\circ$  is estimated from proper motion measurements of approaching and receding ejecta during an outburst, combined with the newly-determined parallax distance of 8.6 kpc (Reid et al. 2014). The method is described in Section 2.1 and pictorially by the schematic in Figure 3. The details of an actual calculation are described in Section 2.3.

## 2.1. A Model of Jet Decay

In this subsection, we motivate a model of the fading compact jet associated with the decay curves in Figure 2. Note that the fading compact jet has never been imaged by VLBA. The full force compact jet has been imaged (see below), but the decay afterwards is determined only by the light curves in Figure 2. Thus, we need some information to guide a necessarily speculative model of how a compact jet fades.

In the context of the decay curves in Figure 2, the flux density decays to low levels, but not zero. Thus, we expect a low surface brightness jet is the end state. There are some compact jet states that end with a major ejection. This is in distinction to the fade seen here. In this case, the compact jet either disappears or is too weak to be detected with a low sensitivity VLBA observation (Dhawan et al. 2004).

The fading of the compact jet or the disappearance of the compact jet is assumed to represent a decrease in the intrinsic power of the compact jet. The interior of the jet is hidden by synchrotron self-absorption (SSA). The emission that is detected at 15 GHz is the  $\tau \sim 1$  surface of the outgoing plasma. We assume that the power is drastically reduced on a time scale,  $T_0$ , much shorter than the time it takes the plasma to flow a scale length for

the jet that represents a large fraction of the detected emission with VLBA,  $L$ . The abrupt transition to a state of highly reduced jet power begins at  $t = 0$  and proceeds to completion in the time interval  $0 < t < T_0$ . In the examples to follow,  $L > 2$  mas. Namely, if the plasma velocity is  $V$ , then  $VT_0 \ll L$ . This seems like a reasonable assumption considering that the jet originates from a region near the black hole that is seven orders of magnitude smaller than the jet length,  $L$  (Punsly 2011). After the transition, a very weak jet is ejected from the central engine at  $t > T_0$ . However, there is still plasma from  $-L/V < t < 0$  that occupies the conduit of the original HPS jet. The plasma that flows down this conduit is a strong transient feature that is approximately a step wave. In the language of magnetohydrodynamics this is approximately a contact discontinuity (not a shock wave) that propagates at the speed,  $V$ , of the bulk flow of the jet plasma if the plasma is turbulent. The discontinuity might have to be supplemented by a more complicated rarefaction wave structure in principle, but this detail will not affect the emissivity and velocity of the preponderance of the remnant plasma from the HPS steady jet which is far upstream of the disturbance. The abrupt change that is assumed to occur is the fundamental assumption of the model of the jet fading that is manifest as a large transient discontinuity.

The plasma upstream of the propagating discontinuity has virtually the same plasma properties as the plasma ejected at  $t < -L/V$  that was located at this same axial coordinate,  $x$ , along the jet during the steady HPS jet state. This includes the number density of particles and the magnetic field strength. The SSA opacity is determined by the local plasma state and is therefore virtually the same as it was at  $t < -L/V$  during the steady jet phase of the HPS (Ginzburg and Syrovatskii 1969). The region for which this is true changes with time and is defined by the axial coordinate range,  $x > Vt, t > 0$ . For this portion of the jet, the  $\tau \sim 1$  surface and the intrinsic emissivity is virtually unchanged from the HPS steady jet. For  $x < Vt, t > 0$ , the jet will be the weak new jet that was emitted from the central engine. Of course, an abrupt step function change is a mathematical simplification, but the transition region is much thinner than  $L$ . The change in emissivity is so drastic that for  $t < L/(2V)$ , the older plasma at  $x > Vt, t > 0$  is much more luminous than the newer plasma at  $x < Vt, t > 0$  and this dominates the integrated jet luminosity. Based on Figure 2 (and as verified in the analysis to follow) this describes the jet evolution and emissivity for many hours. At late times, a new weak jet may form and this is likely to have a more compact  $\tau \sim 1$  surface since the number density and magnetic field are likely less. However, this is after the decay and is not germane to the discussion of the prompt decay of the 15 GHz flux density.

In summary, we are looking for a model of jet fading that is a consequence of a drastic reduction in jet power and in general leaves a weak jet behind. This simple model is a propagating discontinuity that separates the strong jet region from the weak jet region.

Figure 3 describes our model. We emphasize that the simple dynamic depicted has never been directly observed. However, it is consistent with what we know about the compact jet from VLBA imagery and radio light curves. In Figure 3,  $t = 0$  on the left indicates a steady HPS jet, the type of jet that we will describe later in Figures 4 and 5 and has been observed with VLBA (Fuchs et al. 2004; Ribo et al. 2004). The 4 steps in the grey scale shading crudely indicate the decay of luminosity along the jet length. The darker the grey, the brighter the jet. The power source for the jet is suddenly diminished in strength at  $t = 0$ , except for a weak (light grey) jet that persists during the event. For the sake of argument, the weak background residual jet has an integrated 15 GHz flux density  $\sim 10$  mJy while the HPS jet was originally  $\sim 100$  mJy. The high emissivity plasma continues to propagate down the conduit formed by the steady state HPS jet after  $t = 0$ . The transition from light grey below to darker grey above locates the position of the discontinuity in the snapshots  $\geq 2$  hrs. As it propagates, the plasma upstream obeys the same effective emissivity (the resultant emissivity that includes the effects of Doppler beaming and SSA applied to the intrinsic emissivity) profile as the HPS steady state jet in this region as determined empirically from the VLBA radio images. The original dark grey rectangle has moved downstream towards the top of the figure and occupies the position of the fainter second rectangle at  $t = 2$  hrs. The next time step proceeds similarly. No new flow of high emissivity jet material leaves the central engine, the central engine for the jet is still nearly shutoff. The high emissivity plasma that once occupied the lowest rectangle at  $t = 0$  continues advancing towards the top of the figure and occupies the third position at  $t = 4$  hrs. The jet luminosity decay continues and this is represented by the lighter shade of grey.

## 2.2. Previous Models of Compact Jets

One approach to describing the jet spatial variation is based on simple theoretical jet models. These were introduced into the literature in Blandford and Königl (1979) which give some general features of the effects of synchrotron self-absorption (SSA) and beaming in jets. However, these power law models of the parameters were found to be too simplistic to describe astrophysical jets and more elaborate power law depictions of jets were created to deal with the constraints imposed by observation (Ghisellini et al. 1985; Ghisellini and Maraschi 1989; Ghisellini et al. 1996). These models were developed for extragalactic radio sources. Similar types of power law models for Galactic sources were applied to the jets in Cygnus X-1 and MAXI J1659-152 (Kaiser 2006; Paragi et al. 2013).

In the context of GRS 1915+105, models based on Ghisellini et al. (1985); Ghisellini and Maraschi (1989); Ghisellini et al. (1996) were applied to the compact jet (Punsly 2011). The mod-

els described the surface brightness profile of the compact jet considered here (in the next subsection and Figure 4) as well as the broadband spectral energy distribution. In order to satisfy all of the constraints of the observations, the jet models were necessarily highly stratified in the transverse direction. The inner most jet was the most collimated and the magnetic field was turbulent in equipartition with the plasma energy. The magnetic field became ordered outside of this core and the jet expanded more rapidly with increasing transverse distance from the core. The jet flared non-uniformly in the axial direction as well. In the end, the parametric jet had 55 input parameters describing the various power laws.

Power law models incorporate the intrinsic luminosity, SSA, Doppler beaming and the basic dimensions to create an effective emissivity. The complexity of the parametric model is not essential to understand in the present context. In order to implement the model of the compact jet from the last section, we are striving to understand the spatial variation of the effective emissivity of the steady state HPS jet. In this regard, it is not advantageous to assume that actual jets are well described by numerous parameters that obey power laws. This has no benefit in the present context and we strive to find something directly related to the observations. Instead, we choose to empirically determine the spatial variation of the source of effective emissivity responsible for the images of the compact jet in Fuchs et al. (2004); Ribo et al. (2004) during HPSs. Namely, we want to determine the source function for the effective emissivity directly from the radio images, independent of the theoretical model of the jet.

### 2.3. An Empirical Source Function for the Compact Jet

There have been two deep 15 GHz VLBA (milliarcsecond - resolution) observations of a HPS compact jet that have been published. The first, was reported in Fuchs et al. (2003, 2004) and occurred on MJD 52731.6, 1.6 days before the HPS decay chronicled in the top frame of Figure 2. The second occurred on MJD 52748.4 (Ribo et al. 2004). We note that compact jets were observed in Dhawan et al. (2000), but these were not HPS jets. We comment on these observations at the end of this section. In order to estimate  $D$ , the total flux density as a function of displacement along the approaching jet is calculated from the radio image. The result of this integration for MJD 52731.6 is the black curve plotted in the left hand frame of Figure 4. This is the “steady” state before the decay. The curve is the cumulative distribution of the detected 15 GHz flux density along the approaching jet. It begins as 0% at the radio core and equals 100% at the last contour in the radio image. The fact that this is not the actual end of the jet is not significant since the flux density is greatly reduced at these distances. The next step is to make a comparison with a radio

luminosity source function. In order to do this we note three major facts

1. The jet is unresolved along its width so the source of effective emissivity for the VLBA image can be represented by a line source
2. It should be noted that this image is blurred (made longer) by the finite beam-width of the interferometer and interstellar scintillation. Based on the results of Dhawan et al. (2000), it is estimated that effective “blurred beam-width” (that includes the effects of interstellar scintillation) is 1.54 mas. The actual jet is effectively viewed through this “blurring aperture.”
3. One other caveat is that the brightness of the jet within the vicinity of the radio core depends on the jet velocity. The finite resolution of the interferometer will detect emission from both the counter-jet and the approaching jet in this region. The observed flux density,  $F_\nu \sim \nu^{-\alpha}$ , in any beam is a Doppler enhancement of the intrinsic flux,  $F_{\text{intrinsic}}$  (Lind and Blandford 1985):

$$F_\nu = \delta^{2+\alpha} F_{\text{intrinsic}} , \quad (2)$$

where

$$\delta = \frac{\sqrt{1 - (v/c)^2}}{1 - (v/c) \cos \theta} . \quad (3)$$

Equation (2) provides an enhancement of the approaching jet flux and a reduction of the receding jet flux. The net effect of Equation (2) and the finite resolution of the restoring beam is to produce a velocity dependent offset of the peak of the flux density of the radio image from the true core position. The 1.54 mas effective beam width centered on the peak flux will detect major fractions of both the approaching and receding jets. The core shift is needed to allocate proper amounts of the peak flux density to each side of the jet. The fraction of core flux assigned to the approaching jet by the implementing a core shift from the flux peak will be equal to the fraction of the total jet flux in the approaching side - if bilateral symmetry holds and the jet has a constant velocity. This offset is required to identify a starting point for the cumulative flux distribution of the approaching jet as observed with VLBA (the black curve in the left frame of Figure 4). Yet, the resultant decay length  $D$  that arises at the end of the analysis (combined with the decay time,  $T$ ) must also produce the same velocity used in the derivation of the offset. So the problem is nonlinear. For example, in the analysis of this paper, the peak flux per beam is offset downstream of the true core position by  $\approx 0.3$  mas. In order to understand this core shift concept, and to appreciate the nonlinearity, we verify that it is of the correct magnitude explicitly after Equation (6).

We are actually interested in the empirical source function for the emissivity that was emitted by the source (not the image blurred by scatter-broadening and the finite resolution of the VLBA) in order to understand the length scale over which physical changes take place. We have created such an empirical source function and then mathematically blurred the image in order to replicate the image made by VLBA. The resultant cumulative distribution of flux density of the approaching jet is plotted as the red curve in the left hand side of Figure 4. We can write the empirical source function,  $S(x)$ , for the effective emissivity as

$$S(x) = (F_0/D)e^{-x/D}\delta(v)^{2+\alpha}\Theta(x) + (F_0/D_{\text{rec}})e^{x/D_{\text{rec}}}\delta(-v)^{2+\alpha}\Theta(-x) , \quad (4)$$

where  $x$  is the actual axial displacement of the jet plasma from the radio core and  $\Theta(x)$  is the Heaviside step function. The first term represents the approaching jet,  $D$  is the e-folding distance and  $F_0$  is the normalization. The second term is the source function of the receding jet. This is required because the wide effective beam width of the observation samples the receding jet as well near the origin of the approaching jet. We have introduced  $D_{\text{rec}}$ , the e-folding distance of the linear source function for the effective emissivity of the receding jet. In order to transform this quantity to the observed emissivity,  $\mathcal{E}(y)$ , one must convolve with a Gaussian beam. If  $y$  is the observed displacement from the radio core,

$$\mathcal{E}(y) = \int_{-\infty}^{\infty} S(x) \frac{1}{\sqrt{2\pi}\sigma} e^{-\frac{(x-y)^2}{2\sigma^2}} dx , \quad (5)$$

where the standard deviation,  $\sigma$ , is the effective beamwidth (1.54 mas) divided by 2.35 (the factor required to convert full width at half maximum to standard deviation). The radio images were made from a circular beam. The cumulative distribution,  $\mathcal{F}(y)$ , that is plotted in red in Figure 4 is

$$\mathcal{F}(y) = \frac{\int_0^y \mathcal{E}(z) dz}{\int_0^{\infty} \mathcal{E}(z) dz} . \quad (6)$$

At this point it is easier for the reader to appreciate the core shift discussed in item (3) above. The empirical jet starting point is ambiguous since this inherently asymmetric source is sampled by a very wide effective beam (compared to the proper size of the core). The effective beam (including interstellar scintillation) is 1.54 mas (compare this to the e-folding distance derived by this analysis of 1.2 mas in Figure 4). Thus, the beam is large compared to the characteristic dimension of the jet. When the beam is centered on the peak flux density ( $F_{\nu}(\text{peak})$ ) location, it is capturing flux density from both the approaching ( $F_{\nu}(\text{core app})$ ) jet and the receding ( $F_{\nu}(\text{core rec})$ ) jet. We can write this as

$$F_{\nu}(\text{peak}) = F_{\nu}(\text{core app}) + F_{\nu}(\text{core rec}) . \quad (7)$$

We have two constraints. From Equation (2) and the assumption of bilateral symmetry

$$\frac{F_\nu(\text{core app})}{F_\nu(\text{core rec})} = \frac{\delta(v)^{2+\alpha}}{\delta(-v)^{2+\alpha}} . \quad (8)$$

We use the value of  $\alpha = 0.1 \pm 0.2$  for the jet on MJD 52731.6 that was previously determined from VLBA images (Ribo et al. 2004). The other constraint derives from the constant velocity assumed for the jet which leads to the approximately constant Doppler enhancement along the jet from Equations (2) and (3) if  $\alpha \approx 0$ , as observed. Thus, the total jet integrated flux density fractions in the approaching and receding jets should be approximately the same as the ratio of flux density from the core assigned to the approaching and receding jets

$$\frac{f}{1-f} \equiv \frac{F_\nu(\text{total jet app})}{F_\nu(\text{total jet rec})} \approx \frac{F_\nu(\text{core app})}{F_\nu(\text{core rec})} = \frac{\delta(v)^{2+\alpha}}{\delta(-v)^{2+\alpha}} . \quad (9)$$

The next thing that needs to be computed is the effective core offset in the radio image that assigns a fraction,  $f$ , of the peak flux density to the approaching jet and a fraction,  $1-f$ , of the peak flux density to the receding jet. We need this offset in order to know exactly where to start the integration of the cumulative approaching jet flux density that is computed in the left hand side of Figure 4. From item (1), a line source for the effective emissivity is consistent with the data. Therefore, we can approximate the offset,  $\Delta$ , of the start of the approaching jet from the center of the beam located at the point of peak flux density as

$$\Delta \approx \frac{F_\nu(\text{core app})}{F_\nu(\text{peak})}(1.54 \text{ mas}) - 1.54 \text{ mas}/2 \approx (f - 0.5)1.54 \text{ mas} . \quad (10)$$

As an example, if one were to split the core evenly with both the receding jet and approaching jet then  $f \approx 0.5$ . The jet would begin with zero offset, i.e. both the jet and counter jet start at the point of peak flux density. By Equation (9), this corresponds to  $v \approx 0$ . This linear approximation for the offset is only accurate if the beam is much wider than the size of the magnitude of the offset.

One can now appreciate how nonlinear an iterative solution is in general. One has five constraints, Equation (6) for both the jet and counter jet, the left hand and right hand equalities for the flux ratio in Equation (9) and Equation (10), and five unknowns  $v$ ,  $D$ ,  $D_{rec}$ ,  $f$  and  $\Delta$ . Thus, a solution should exist if the model is a reasonable representation of the physical situation. Trial values of  $v$ ,  $D$ ,  $D_{rec}$  and  $\Delta$  must be chosen. The value of  $\Delta$  determines the start point of the integration of the jet and counter jet flux densities over their respective lengths. Using this starting point, one can compute the total flux density in both the approaching and receding jets,  $F_\nu(\text{core app})$  and  $F_\nu(\text{total jet rec})$ , respectively. From Equation (9) this determines  $f$  which in turn determines  $\Delta$ , by Equation (10), hence the

first aspect of the nonlinearity inherent to this problem. The other aspect of nonlinearity of this problem is that the chosen values of  $v$  (the Doppler boosting of both the jet and counter jet),  $D$ ,  $D_{rec}$  in conjunction with Equation (6) needs to produce a cumulative flux density distribution that fits the observed cumulative flux density distribution determined from the VLBA observations. The observed cumulative flux density distribution determined from the VLBA observations is not independent of  $\Delta$  (i.e.,  $\Delta$  changes the origin of integration). So, one is looking not just for an arbitrary solution for  $f$  and  $\Delta$ , but one that can be fit with the simple exponential empirical model. Arbitrary values of  $\Delta$  tend to produce observed cumulative flux density distributions determined from the VLBA observations with non monotonic curvatures which are poorly fit by the exponential model. A third nonlinear aspect occurs when any of the parameters  $v$ ,  $D$  or  $D_{rec}$  are varied in the process of finding a solution, the other two parameters must be changed in order to fit the data due to the large beam size which captures both the approaching and receding jets near the core. Many iterations are required before agreement of the constraints are reached.

Note that the method above is not guaranteed to produce a good fit if the empirical model is inherently inaccurate. However, we have found some rather tight fits to the data. Our best fit is shown on the left hand side of Figure 4. The parameters are  $D = 1.2$  mas for the approaching jet. This model also required  $v = 0.35c$ , which corresponds to an apparent velocity of the approaching jet of  $V_{app} = 0.36c$ . A similar fit to the receding jet yielded  $D_{rec} = 0.6$  mas, consistent with the foreshortening of the receding jet that is readily visible in the radio image. The velocity  $v = 0.35c$  corresponds to an apparent velocity of the receding jet of  $V_{app} = -0.25c$ . The fraction of the flux in the approaching jet was found self-consistently to be  $f \approx 69\%$ . This agrees with the results of Ribo et al. (2004), but agreement need not occur in general (see Figure 5 and the related discussion). The offset of the peak flux relative to the start of the jet is  $\Delta \approx 0.3$  mas.

As an aside, we note that Equation (10) is not the same calculation as the core offset due to SSA (Blandford and Königl 1979). We are not comparing core positions at different frequencies as in a discussion of SSA opacity. We are estimating the fraction of the peak flux in the very wide beam (compared to the size of the jet) that is attributable to the approaching jet at one frequency, 15 GHz. Certainly, there is a relationship between the two ideas, and the offset estimate in Equations (7) - (10) can be considered a crude independent method of estimating the magnitude of the shift in position of the origin of the jet relative to the peak of the flux density as is the intent of SSA core shift analysis. This method requires

- a knowledge of the angle of the jet to the line of sight,
- the velocity of the jet and counter jet ,

- a detected jet and counter jet,
- and a constant spectral index along the jet.
- the effective beam width is comparable to the spatial scale of variation (eg.,  $D$ )
- the effective beam width is much larger than the computed offset
- The jet and counter jet are unresolved in the transverse direction

The method assumes that

- the velocity is constant along the detected jet and counter jet,
- intrinsic bilateral symmetry,

In general, one does not have sufficient astrometric accuracy and numerous high frequencies of sampling in order to accurately find the core position by extrapolating the core shift to infinite frequencies (in the SSA based method). Equations (7) - (10) can provide a crude estimate of the core shift if the seven requirements listed above are achieved.

The computation of  $V_{app}$  is based on  $D$ , the e-folding distance of the linear source of effective emissivity. We now invoke the model of the flare decay posited in Section 2.1 and illustrated in Figure 3. This model is equivalent to identifying the time dependent line source for the effective emissivity of the approaching jet,  $S_{app}(x, t)$ , after the central engine power has been drastically reduced as

$$S_{app}(x, t) = S_0(0.7/D)e^{-x/D}\Theta(x - V_{app}t) + \epsilon(x)\Theta(x) , \quad (11)$$

where  $\Theta(x - V_{app}t)$  is the Heaviside step function and  $\epsilon(x)$  is the low level background residual jet (i.e., the jet does not turn all the way off in general).  $S_0$  is the overall normalization. The coefficient of 0.7 results from the fact that 70% of the 15 GHz flux in the jet 1.6 days earlier (on MJD 52731.6, the left hand frame of Figure 4) is in the approaching jet and 30% in the receding jet (Ribo et al. 2004). We assume this same fraction. The light curves in Figure 2 represents the total integrated luminosity. Therefore, we need the contribution from the receding jet as well. For the receding jet, one has

$$S_{rec}(x, t) = S_0(0.3/D_{rec})e^{x/D_{rec}}\Theta(-x + V_{rec}t) + \epsilon_{rec}(x)\Theta(-x) . \quad (12)$$

Assuming bilateral symmetry in Equation (1) and a line of sight of  $60^\circ$  (i.e.,  $-120^\circ$  for the receding jet) determined in Reid et al. (2014), the receding apparent velocity is  $V_{rec} = -0.25c$ .

At any time  $t$ , after the jet central engine was reduced in power, the total flux density,  $F_\nu$ , emitted from the compact jets is

$$F_\nu(t) = \int_{-\infty}^{\infty} S_{\text{app}}(x, t) + S_{\text{rec}}(x, t) dx \approx 0.7S_0 e^{-V_{\text{app}}t/D} + 0.3S_0 e^{V_{\text{rec}}t/D_{\text{rec}}} . \quad (13)$$

The exponential line source from Equation (4) for the effective emissivity with an e-folding distance for the approaching (receding) jet of  $D = 1.2$  mas ( $D_{\text{rec}} = 0.6$  mas) and a bulk velocity  $V_{\text{app}} = 0.36c$  applied to Equations (11) - (13) can be used to quantify the simple fading jet model of Section 2.1. Equation (13) yields the fit to the decay data presented in Figure 2 in the right hand side of Figure 4. We plot the curve two ways in order to investigate the affect of shifting the origin of time. The solid red curve is a plot of the decay if it started when the observation started. The overall normalization is  $S_0 = 94$  mJy. The heavy dashed black curve has a starting flux density of 135 mJy when the decay started, similar to the level the day before (see Figure 2). This requires that the observation started 1.2 - 1.4 hrs before the observation in order to achieve a good fit. The decay is not that sensitive to the start time for an exponential decay as can be seen from Equation (13). The larger term from the approaching jet is also from the longer jet with the larger decay time, so this larger exponential function dominates more as time elapses and the decay gets closer to a pure exponential. There is a slight excess at late times to the fit in the right hand side of Figure 4, this might represent emission from the weak new jet. In summary, this empirical source function for the effective emissivity reproduces the compact jet in the HPS on MJD 52731.6 and (in the context of the simple jet fading model) the subsequent decay on MJD 52733 just 1.6 days after the jet was imaged.

Even though a major advantage of studying HPS is to provide a stable state to analyze, it should be noted that in general 1.6 days is a long time interval for dynamic change in GRS 1915+105. Major changes can occur in the X-ray and radio on time scales of seconds or minutes (Klein-Wolt et al. 2002). Although, we have no evidence that this occurs in HPS, it might not be valid to assume that the  $D$  value determined in Figure 4 typified the jet just prior to the decay. Without simultaneous data, this can only be estimated by studying multiple VLBA images of HPS. This is addressed below.

The most sensitive radio imaging of an HPS jet was on MJD 52748.4 (Ribo et al. 2004). Figure 5 shows the fit of a linear decaying source of the effective emissivity to the cumulative flux distribution along both the approaching and receding jets. The fit is defined by  $D = D_{\text{rec}} = 1.5$  mas and  $v = 0.15c$ . This jet is much more symmetric than the jet on MJD 52731.6 and therefore requires a much smaller bulk velocity. The decay length is slightly larger than that on MJD 52731.6 in Figure 4. There is one interesting feature that is unique to this radio image. A weak discrete ejection appears from 2 to 4 mas beyond the end of the compact jet.

Comparing with the 8.3 GHz radio image in Ribo et al. (2004) indicates that it is optically thick (flat spectrum). The feature is 10 times the rms noise in the image and seems to be real, but without a deeper image showing a similar feature we cannot rule out this as an artifact of inadequate u-v coverage. Thus, we must consider this a tentative detection of a discrete component. A third unpublished HPS compact jet observation with comparable u-v coverage and sensitivity to the two images analyzed in this paper was also performed<sup>1</sup> and occurred on MJD 52722 and is also consistent with  $D \approx 1.2 - 1.5$  mas.

The range of  $1.2 \text{ mas} < D < 1.5 \text{ mas}$  is consistent with the two other 15 GHz VLBA published observations of compact jets with comparable u-v coverage, flux density and sensitivity on MJD 50914 and MJD 50935 (Dhawan et al. 2000). However, these jets were not produced during a HPS. It is worth noting that the much weaker (45 mJy) compact jet observed on MJD 50744 reported in Dhawan et al. (2000) was fit with an e-folding distance of  $< 1$  mas. This small value might be an artifact of the insufficient sensitivity to detect the faint jet extremities.

The 1.6 days between the VLBA observation on MJD 52731.6 and the decay on MJD 52733, is quite long for GRS 1915+105, so one cannot assume that this was the jet length during the decay as noted above. From Figure 2, the e-folding time is bound by the existing observations by  $3.8 \text{ hrs} < T < 8.6 \text{ hrs}$ . From Figures 4 and 5 and the discussion that followed  $1.2 \text{ mas} < D < 1.5 \text{ mas}$ . Then from Equation (1), this creates a range of apparent jet velocities,  $0.16c < V_{app} < 0.46c$  and a range of intrinsic jet velocities of  $0.17c < v < 0.43c$ . The high end of the range is corroborated by other data. It is driven by the rapid decay on MJD 52733 of only 3.6 hrs. It is very likely that this rapid decay is the result of this being a high velocity jet state. It was noted in Ribo et al. (2004) that this was the most asymmetric compact jet ever detected. Thus, their analysis of jet speed from Doppler asymmetry produced the largest  $v$  of any compact jet by a considerable amount. Correcting their result for the new line of sight (see the Discussion) from the parallax measurements of Reid et al. (2014), yields  $v = 0.37 \pm 0.04c$ , in agreement with the maximum estimated  $v$  attained in this study. Another argument for this being the high end of the velocity range is that Table 1 indicates that this HPS was much more luminous than any other observed HPS.

---

<sup>1</sup>Ribo et al. (2004) unpublished result presented at the EVN Symposium 2004 The 7th European VLBI Network Symposium on New Developments in VLBI Science and Technology Toledo, Spain, 2004 October 12-15)

## 2.4. Comparison to Alternative Models of Jet Fading

A key assumption of this study is the scenario for jet fading described in Section 2.1 and illustrated schematically in Figure 3. In this scenario, the jet fading is a transient decay of a strong jet that was abruptly suppressed at its source. There is no direct observational evidence to support this idea and the scenario is not unique. Alternatively, one might think of the jet fading as a slow turnoff of the jet source in which one of the steady state power law solutions of Punsly (2011) is slowly varied and no strong transient or contact discontinuity is created. The lone restriction here is that the plasma from the full power jet episode must propagate sufficiently far down the jet so that its contribution to the total flux density is negligible after an e-folding time  $T$ , i.e  $V_{app} \gg D/T \approx 0.36c$ . If this were not true there would have to be a conspiratory connection between turning down the power source at the base of the jet and the rate that previously ejected high emissivity plasma is losing its surface brightness in order to produce an exponential decay in time - not only once but on both MJD 52733 and on MJD 53122.

In order to assess the plausibility of these ideas, we first note the nontrivial successes of the jet fading scenario presented here:

1. The model provides a physical connection between the spatial exponential decay profile of the source of effective emissivity of the steady state HPS jet and the temporal exponential decay of the fading of the jet emission 1.6 days later
2. The constraint imposed by the above physical connection implies a jet velocity that agrees very closely with the jet velocity found in Ribo et al. (2004) by considering jet bilateral asymmetry due to Doppler aberration of an intrinsically bilaterally symmetric system

By contrast, consider these issues in the context of a slowly varying jet scenario.

1. The spatial exponential decay profile of the source of effective emissivity of the steady state HPS jet and the temporal exponential decay of the fading of the jet emission 1.6 days later are coincidental. The temporal decay profile is a manifestation of how the local physics at the base of the jet alters the parameters injected into the jet model. It is coincidental that this follows an exponential profile on both MJD 52733 and on MJD 53122.
2. The constraint,  $V_{app} \gg D/T \approx 0.36c$  noted above (that is required to produce the temporal exponential decay) disagrees with the jet velocity found in Ribo et al. (2004)

by considering jet bilateral asymmetry due to Doppler aberration of an intrinsically bilaterally symmetric system

One other curious feature of the slowly varying jet scenario is evident if the details of the power law models of Punsly (2011) are considered. The base of the jet that produces the majority of the 15 GHz flux density is located  $< 3 \times 10^7$  cm from the central black hole (see Table 1 and Figure 2 of Punsly (2011)). Considering the time scales for decay of 3.8 hrs and 8.6 hrs from Figure 2, turning down the power of the jet by moving plasma in the disk at the base of the jet corresponds to a rather suspect slow radial velocity of  $\sim 10^3$  cm/s.

In summary, the transient model implies one value of  $V_{app}$  that is consistent with the cumulative flux distribution, the rate of compact jet decay and the bilateral asymmetry. The slowly varying jet model is not consistent with bilateral asymmetry and the variations in time and space are unrelated observable parameters. We choose to consider the interpretation that has descriptive power and is more consistent with other observations, although we can not rule out the slowly varying jet model.

### 3. X-ray Properties of the Decay of High Plateau States

The decay of the HPS on MJD 53122 in Figure 2 was accompanied by Rossi X-ray Timing Explorer (RXTE) observations. Both PCA (Proportional Counter Array) and HEXTE (High Energy X-ray Timing Experiment) observations were performed on MJD 53122.107 and again on MJD 53122.179. For the sake of exploring the time evolution of the disk - jet system, we reduced these data plus the data from the height of the HPS 5 days earlier on MJD 53117.114.

#### 3.1. Observations and Data Reduction

In order to characterize the source X-ray behavior during the HPS, we looked at data that were simultaneous with the HPS that is best followed at radio frequency. We reduced and analyzed Rossi X-ray Timing Explorer (RXTE)/Proportional Counter Array (PCA) data taken during observations that began on MJD 53100.230, 53117.114, 53122.107, 53122.179.

The data were reduced in a very standard manner (as in e.g. Rodriguez et al. (2008)) with the HEASOFT V6.16 software suite. Energy spectra were obtained from the top layer of the Proportional Counter Unit (PCU) #2, background spectra were produced from the

“bright source” model, and responses produced with `pcarsp` for the appropriate PCU, layer and anode. We added 0.6% systematic uncertainties to all spectral channels, and we analyzed the resultant spectra within `XSPEC` v12.9.0.

High resolution ( $7.8125 \times 10^{-3}$  s) light curves covering the full PCA spectral range were obtained from different data modes in different observations. On MJD 53100.230, we used the `GOOD XENON` data, while for the other three observations we combined `BINNED` and `EVENT` that respectively cover the low (0–35 or  $\sim 2 - 15$  keV) and high (36–255,  $> 15$  keV) spectral channels. PDS from each individual observation were produced with `POWSPEC` on intervals of 64 s, all intervals were further averaged.

### 3.2. Results

In order to see the spectral evolution, we show a plot of the spectral energy distributions (SEDs) in the top frame of Figure 6. The first epoch is MJD 53117.114 in red, which occurs during a HPS (see Figure 1). It is a much harder spectrum than the two spectra obtained on MJD 53122.107 (green) and MJD 53122.179 (blue) during the decay of the same HPS (see Figure 2). The plot shows that the spectral softening appears to continue between MJD 53122.107 and MJD 53122.179.

The spectral evolution can be formally characterized by parametric spectral fits. We tried models that required an accretion disk, to look for signs of spectral evolution, but there is no evidence of a disk in any of the data. Our model had the following parameters. The absorbing column of neutral hydrogen,  $N_H$ , was allowed to vary for MJD 53122.107 and MJD 53122.179, in the models described in Table 2, we found values of  $5.69 \pm 0.27 \times 10^{22} \text{cm}^{-2}$  and  $5.88 \pm 0.26 \times 10^{22} \text{cm}^{-2}$ , respectively. Since the values were similar, we fixed  $N_H = 5.7 \times 10^{22} \text{cm}^{-2}$  for MJD 53117.114 which constrained the power law better in the more complicated fit for this epoch in Table 2. We note that if  $N_H$  was left free in the fit on MJD 53117.114, it optimized at  $N_H = 6.3 \times 10^{22} \text{cm}^{-2}$ . Columns (2) - (4) of Table 2 describe the properties of the Gaussian line used in the fit. Columns (5) and (6) are the cutoff energy and e-folding energy required by the fit, respectively. The particle number density power law spectral index,  $\Gamma$ , is tabulated in Column (7). The epoch MJD 53117.114, during the

Table 2: X-ray Spectral Fits

1	2	3	4	5	6	7	8	9	10	11
Epoch	Line	Line	Line	E	E	Power	Power	Flux	Flux	Reduced
Date	Center	Sigma	Norm	Cutoff	Fold	Law	Law	$10^{-8}$	Intrinsic	$\chi^2$
(MJD)	keV	keV		keV	keV	1	2	ergs/s/cm <sup>2</sup>	$10^{-8}$ ergs/s/cm <sup>2</sup>	(dof)
53117.114	$5.86 \pm 0.10$	$1.61 \pm 0.08$	$0.13 \pm 0.01$	$13.9 \pm 0.2$	$25.4 \pm 1.0$	$2.11 \pm 0.06$	$0.54 \pm 0.69$	$2.12 \pm 0.03$	$3.15 \pm 0.05$	1.46(100)
53122.107	$5.69 \pm 0.27$	$1.24 \pm 0.10$	$0.08 \pm 0.01$	$14.3 \pm 0.4$	$34.9 \pm 2.9$	$2.51 \pm 0.02$	...	$2.14 \pm 0.03$	$3.80 \pm 0.06$	1.00(96)
53122.179	$6.29 \pm 0.13$	$1.10 \pm 0.10$	$0.08 \pm 0.01$	$14.7 \pm 0.4$	$35.2 \pm 1.8$	$2.55 \pm 0.02$	...	$2.14 \pm 0.03$	$3.80 \pm 0.06$	1.30(87)

HPS, has a high energy excess and requires a second power law that is poorly constrained by the data, as is indicated by the large relative uncertainty in column (8). The hard second power law comprises only 1.5% of the flux from 1.5 - 150 keV (extrapolated down to 1.5 keV). The total observed flux from 1.5 - 150 keV (extrapolated down to 1.5 keV) is listed in column (9). The intrinsic flux (corrected for  $N_H$ ) from 1.5 - 150 keV is tabulated in column (10). The reduced  $\chi^2$  and degrees of freedom of the model is in the last column. The most striking evolution of the X-ray spectrum from the fully powered up jet state to the jet decay is provided by the spectral index of the underlying power law in column (7). The power law steepens from  $\Gamma = 2.11$  to  $\Gamma = 2.55$ . Perhaps the best way to characterize the steepening of the X-ray spectrum during the jet decay is by looking at the intrinsic flux ratio,  $R = F_{1.5-3}/F_{12-50}$ , where  $F_{1.5-3}$  is the intrinsic flux in the interval 1.5 keV - 3 keV and  $F_{12-50}$  is the flux in the interval 12 keV - 50 keV. The fluxes were computed from PCA observations with the assumption (in contrast to Table 2) that  $N_H = 5.7 \times 10^{22} \text{cm}^{-2}$  and models otherwise similar to those described in Table 2. The fluxes below 2.5 keV were extrapolated from the model and would not accurately depict any low energy contribution from a thermal disk component. These data reductions and extrapolations were originally performed in Punsly and Rodriguez (2013a) as part of a method that calibrated counts from the RXTE All Sky Monitor with PCA determined fluxes. On MJD 53117.114,  $R = 0.42$  compared to  $R = 1.14$  on MJD 53122.179. This softness ratio,  $R$ , is plotted during the course of the HPS and during its decay in the bottom frame of Figure 6. There is a dramatic change during the decay. Considering the top frame of Figure 6, this affect is driven primarily by a change in the soft X-ray flux. The physical interpretation would seem to be that there are less low energy Comptonizing electrons in the jet state and more low energy Comptonizing electrons in the decay state.

Figure 7 contains plots of the power spectral density (PSD) on MJD 53117.114 in red with the PSD of the combined data from MJD 53122.107 and MJD 53122.179 in black. Energy in the temporal variations migrates from lower frequency during the HPS to significantly higher frequency during the jet decay. As a reflection of this, the fundamental quasi-periodic oscillation (QPO) frequency changes by a factor of 3.5, from 0.69 Hz to 2.43 Hz. We also plot another PSD during the HPS, on MJD 53100.230. During the entire HPS the QPO fundamental frequency is less than 1 Hz and this frequency dramatically changes during the decay as noted above.

#### 4. Short Time Scale Variability of Radio Emission

Previously, short time scale variability of the 15 GHz flux density has been associated with compact jets, but not during X-ray classes of type  $\chi$ , equivalent to “hard” X-ray spectra (Pooley and Fender 1997; Klein-Wolt et al. 2002; Mirabel et al. 1998). The associated time scales were from 10 - 45 minutes. It is formally difficult to assess the spectral index of the radio emission, because there is a lag between low frequency and high frequency emission cycles. The spectra of strong quasi-periodic radio emission are typically flat or inverted giving the appearance of synchrotron self-absorbed spectra, but at certain times in the cycle the spectrum can appear to be optically thin and steep (Mirabel et al. 1998; Dhawan et al. 2000; Fender and Pooley 2000). Even the stronger periodic emission could be a superposition of “bubbles” at different stages of their adiabatic decay. Each bubble begins flat spectrum and becomes steep spectrum after adiabatic expansion (van der Laan 1966). The important aspect to be noted here is that some of these states have been shown to correspond to a compact jet with VLBA radio images that morphologically appear similar to the jets in HPS (Dhawan et al. 2000). Much weaker levels of radio emission have also been found to vary on much shorter time scales (Prat et al. 2010; Rodriguez et al. 2008). Even though no quasi-periodic radio emission has been found in  $\chi$  states, the similarity in the radio images between jets in HPS and from quasi-periodic events shown in Dhawan et al. (2000) suggests that there is a connection between these phenomena. Likewise, we are interested in the conjecture that the VLBA images of compact jets are deceiving due to insufficient u-v coverage and sensitivity and there are numerous ghost features moving quickly along the jet that are not imaged (Dhawan et al. 2000). If so, there might evidence of these in the time domain. For the quasi-periodic events that were imaged by VLBA that looked similar to the compact jets there is clear evidence of characteristic time scales in the time domain (Dhawan et al. 2000). Thusly motivated, a search for rapid variations in HPS was initiated in order to see these time scales are also generic time scale of variation for compact jets.

First, the magnitude of the fluctuations are quantified. The preliminary step was to compute a linear fit to each of the 95 Ryle observations (those plotted in Figure 1) of the 8 HPS. A residual from the linear fit was computed every instance of data capture, typically every  $\approx 32$  s. The absolute values of the residuals to the linear fits were compiled as the distribution in the left hand frame of Figure 8. The distribution of these fluctuations is well fit by a Gaussian function of mean zero (plotted as a solid red curve) with a standard deviation of 7.7 mJy. The quoted instrumental uncertainty is  $\approx 6$  mJy for the Ryle telescope with 32s integration (Pooley and Fender 1997). Thus, there is possibly a slight excess in these states over the systematic instrumental rms. These are not large fluctuations. One can interpret the residuals from the linear fits to the individual Ryle observations as being distributed as a standard normal distribution. With this interpretation, a simple convolution of standard

normal distributions indicates that the data is consistent with a standard normal distribution of intrinsic fluctuations with a standard deviation  $\lesssim 5$  mJy, i.e.,  $\sigma^2 = \sigma_{\text{systematic}}^2 + \sigma_{\text{intrinsic}}^2 = 6^2 + 4.8^2 = 7.7^2$ . Alternatively, since these are highly luminous states, the systematic error might just be larger. Figure 8 does not show any excess in the tail of the normal distribution. There is no evidence for the large (20 mJy -50 mJy) oscillations that were discussed in Pooley and Fender (1997); Klein-Wolt et al. (2002); Mirabel et al. (1998) for quasi-periodic states.

Secondly, there are 15 observations of over 3 hrs of the HPSs. These are combined to produce the power spectrum in the right hand frame of Figure 8. The power spectrum was computed as the amplitude of the complex Fast Fourier Transform of the auto-correlation function of the ensemble. The normalization is chosen so that the integral of the power over the sampled frequency range ( $5.49 \times 10^{-5}$  Hz to  $1.40 \times 10^{-2}$  Hz) is equal to unity (i.e., the integral of the PSD equals the total power in the fluctuations). In order to interpret the spectrum, we compare it to simple models of noise. To make a comparison to the Fast Fourier Transform result, we compute the complex Fourier integral of the autocorrelation function over positive frequencies then take the amplitude. The power spectrum is well fit by the power spectrum of red noise with a break to white noise at higher frequency (Kittel 1961). To facilitate the comparison requires re-normalizing the red noise spectrum, with a white noise break at high frequency, so that the integral of the composite theoretical power spectrum from  $5.49 \times 10^{-5}$  Hz to  $1.40 \times 10^{-2}$  Hz is unity, the same as the normalization of the ensemble PSD. The fact that the curvature of the red noise spectrum is not captured by the ensemble PSD, does not allow us to create a strong constraint on the characteristic correlation time of the red noise. The only constraint that we have is that the correlation time is  $> 3000$  s. The fit at low frequency is improved for longer correlation times. The PSD transitions from red noise to white noise at frequencies above 0.0056 Hz. There is no excess power associated with the time scales reported for the quasi-periodic radio states in Pooley and Fender (1997); Klein-Wolt et al. (2002); Mirabel et al. (1998). Based on the variability analysis, the compact jets in the HPSs are a distinct phenomenon from quasi-periodic radio events. Whatever the cause of the quasi-periodic variations, these variations are suppressed by the strong compact jet associated with the HPS. There is also no evidence of ghost features in the VLBA images that might be moving with a much larger bulk velocity than was found here. The time domain analysis illustrated in Figure 8 indicates a continuous jet structure with minimal contribution from transient features.

## 5. Discussion

It was shown that two HPS decayed with e-folding times of  $T = 3.8$  hrs and  $T = 8.6$  hrs at 15 GHz. This time scale can be converted to a bulk velocity by considering the 15 GHz VLBA images of three HPS. From these images, after the effective beam-width was de-convolved, the empirically determined source of the effective emissivity for the 15 GHz flux was found to decrease exponentially along the jet direction with an e-folding distance of  $1.2 \text{ mas} < D < 1.5 \text{ mas}$ . Assuming that the power at the base is abruptly diminished significantly and the previously ejected plasma continues down the jetted path, an apparent bulk velocity was estimated as  $V_{app} = D/T$ . It was found that  $0.16c < V_{app} < 0.46c$ . This transforms to an intrinsic velocity  $0.17c < v < 0.43c$ .

We can compare these results to estimates of the bulk jet velocity that arise from Doppler boosting and bilateral symmetry. In Dhawan et al. (2000), it was determined from these arguments that  $v \approx 0.1c$ . In Ribo et al. (2004), using the same assumptions,  $0.27c < v < 0.54c$  based on later compact jet observations with VLBA. These previous treatments assumed a larger angle of inclination,  $\theta = 70^\circ$ . However,  $\theta = 60^\circ$  has now been estimated from proper motion measurements of approaching and receding ejecta during an outburst, combined with the newly-determined parallax distance of 8.6 kpc (Reid et al. 2014). So these older estimates are on the high side by a factor of  $\cos 60^\circ / \cos 70^\circ = 1.47$ . Thus, with the revised distance estimate  $0.18c < v < 0.37c$  based on bilateral symmetry or  $0.07c < v < 0.37c$  if one also includes the Dhawan et al. (2000) results. There is an important assumption in deriving  $v$  in Ribo et al. (2004). The central Clean Component (CC) was always assigned to the approaching jet. This is roughly consistent with the location of the BHXRb being upstream of the peak of the flux density. It was shown in Section 2, based on our exponential line source model fits, that the peak flux density lies 0.3 mas downstream of the beginning of the approaching jet. This is roughly consistent with assigning the central CC to the approaching jet. However, for completeness we note that if the central CC is assigned to both jets or to neither of them,  $v$  decreases to approximately  $0.2c$  using  $\theta = 70^\circ$ <sup>2</sup>. Thus, the independent determination of  $v$  in this paper and the bilateral symmetry arguments provide excellent agreement. It might vary from jet episode to jet episode, but in no case is it relativistic like a radio loud quasar jet or even like the discrete (superluminal) ejections.

The bilateral symmetry argument is more robust when taken as a collected set of data as opposed to each observation individually. If the intrinsic velocity were much larger than indicated by the asymmetry in the images, it is hard to understand how different epochs

---

<sup>2</sup>as communicated by M. Ribo at the EVN Symposium 2004 The 7th European VLBI Network Symposium on New Developments in VLBI Science and Technology Toledo, Spain, 2004 October 12-15

with different u-v coverage and observation durations could consistently produce highly symmetric images. Namely, with many observations, there is no reason to believe that there is somehow always the right amount of missing flux due to poor u-v coverage that skews the bilateral asymmetry to make it appear symmetric. This argument is compelling whether the intrinsic source is actually symmetric or not. Furthermore, our independent method (using exponential decay lengths and times) of estimating  $v$  from the VLBA images implies  $0.17c < v < 0.43c$ , an almost identical range to that implied by estimates from bilateral symmetry based on the same radio images (using the new parallax determined line of sight)  $0.18c < v < 0.37c$  (Ribo et al. 2004). It is concluded that the original bilateral symmetry based estimates of  $v$  from Ribo et al. (2004) are correct or there are numerous conspiring coincidences. The direct implementation of VLBA images to constrain  $v$  is in our opinion superior to folding in information such as time scales of quasi-periodic events (no evidence of quasi-periodicity was found in Section 4) in order to estimate  $v$ .

It is natural to tie the X-ray observations of an HPS during decay in Section 3 to disk models of jet emission in BHXRBs. We concluded that during strong jet emission there was a paucity of low energy Comptonizing electrons. We also noted that the spectral power of X-ray variations was at much lower frequency when the jet is at full force. If one equates lower frequency to large dimensions this suggest a scenario in which the low energy Comptonizing electrons occupy the inner regions of the accretion flow plus corona. When the jet is fully powered up it displaces these electrons. When the jet powers down this region re-fills with low energy Comptonizing electrons. This idea is similar to the unified model of GBH jets of (Fender et al. 2004). The one difference is that instead of the jet displacing the optically thick plasma responsible for the soft thermal emission from the inner disk, the jet is displacing low energy optically thin plasma from the inner regions of the accretion system. We do note that if the disk temperature is too cold for us to identify it in our spectral fits, a thermal disk that approaches the black hole during the decay of the compact jet could also produce these effects.

As promising as a unified picture of GRS 1915+105 jets appeared to be as a laboratory for studying the more distant jets in radio loud quasars (which evolve over time scales much longer than a human lifetime), the popularized notion that Galactic black holes produce highly relativistic jets was tempered by the first parallax distance estimate to GRS 1915+105. Radio-loud quasar jets clearly propagate with highly relativistic bulk velocities. However, the relativistic speed inferred for discrete ejections in GRS 1915+105 was based on crude distance estimates and physical arguments that yielded a distance of 11 kpc - 12.5 kpc. The parallax determined distance measurement is  $8.6^{+2.0}_{-1.6}$  kpc (Reid et al. 2014). This changes the intrinsic velocity of the discrete ejections to  $0.65c$  -  $0.81c$ . As a corollary to this, it was shown that the analogy between the discrete ejections and Fanaroff-Riley II RLQs is

untenable if the distance is less than 10.5 kpc (Punsly and Rodriguez 2013b). We note that the other strong case for direct observational evidence of superluminal motion in a Galactic black hole (GBH), GRO J1655-40, was also based on a crude distance estimate that has been questioned to be much smaller based on newer data and these discrete ejections do not seem to be superluminal (Foellmi et al. 2006). Based on the dichotomy of the types of jetted emission noted in the Introduction, the lack of direct observational evidence of highly relativistic motion in BHXRBs and the lack of an analog with FR II jets indicates that the assumption of relativistic bulk motion in compact jets should be used with great caution. The findings of this study do not support highly relativistic motion in compact jets as well. The analogy between jets in BHXRBs and jets in radio loud active galactic nuclei is not clear.

## REFERENCES

- Belloni, T., Klein-Wolt, M., Mndez, M., van der Klis, M., van Paradijs, J. 2000, *A & A* 355 271
- Blandford, R. and Königl, A. 1979, *ApJ* **232** 34
- Corbel, S. et al. 2000, *A & A* 359 251
- Corbel, S., Nowak, M. A., Fender, R. P., Tzioumis, A. K., Markoff, S. 2003, *A & A* 400 1007
- Dwahan, V., Mirabel, I.F., Rodriguez, L. 2000, *ApJ* 543 373
- Dwahan, V., Muno, M., Remillard, R. 2004, in X-Ray Timining 2003 Rossie and Beyond AIP Conference Proceedings, Volume 714, pp.150-153 (2004)
- Done, C., Wardzinski, G., Gierlinski, M. 2004, *MNRAS* 349 393
- Fender, R. et al., 1999, *MNRAS* 304 865
- Fender, R. et al., 1999, *ApJL* 519 165
- Fender, R. and Pooley, 2000, *MNRAS* 318 L1
- Fender, R., Belloni, T., Gallo, E. 2004, *MNRAS* 355 1105
- Foellmi, C.; Depagne, E.; Dall, T. H.; Mirabel, I. F.. 2006, *A & A* 457 249
- Fuchs, Y. et al., 2003, *A & A* 409 L35

- Fuchs, Y. et al., 2004, Proc. of the 5th INTEGRAL Workshop (ESA)  
<http://xxx.lanl.gov/abs/astro-ph/0404030>
- Gallo, E., Fender, R., Pooley, G. 2003, MNRAS 344 60
- Ginzburg, V. and Syrovatskii, S. 1969, Annu. Rev. Astron. Astrophys. 7 375
- Kittel, C. 1961, Elementary Statistical Physics. (Wiley, New York)
- Ghisellini, G., Maraschi, L. and Treves, A., 1985, A & A 146 204
- Ghisellini, G. and Maraschi, L., 1989, ApJ 340 181
- Ghisellini, G., Maraschi, L. and Dondi, L., 1996, Suppl. Series A & A 120 503
- Kaiser, C. 2006, MNRAS 367 1083
- Klein-Wolt, M. et al., 2002, MNRAS 331 745
- Lind, K., Blandford, R. 1985, ApJ 295 358
- Mirabel, I.F., Rodriguez, L. 1994, Nature 371 46
- Mirabel, I.F. et al.. 1998, A & A 330 L9
- Paragi et al., 2013, MNRAS 432 1319
- Pooley, G. and Fender, R. 1997, MNRAS 292 925
- Prat, L., Rodriguez, J, and Pooley, G. 2010, ApJ 717 1222
- Punsly, B. 2011, MNRAS 418, 2736
- Punsly, B., Rodriguez J. 2013, ApJ 764, 173
- Punsly, B., Rodriguez J. 2013, ApJ 770, 99
- Reid, M. et al.. 2014, ApJ 796 2
- Ribo, M., Dhawan, V. Mirabel, F. 2004, Proc. of the 7th VLBI Network Symposium,  
Bachiller, R., Colomer, F., Desmurs, J., de Vicenete, P. (eds) Toledo, Spain  
astro-ph/0412657
- Rodriguez, J. et al. 2008, ApJ 675 1449
- Rushton, A., Spencer, R.E., Fender, R. and Pooley, G. 2010, A & A 524 29

van der Laan, H. 1966, *Nature* 211 1131

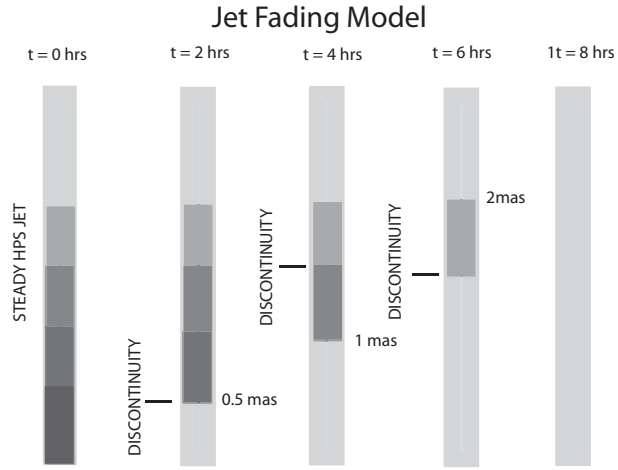


Fig. 3.— The time evolution scenario for jet fading that is described in Section 2.1. The figure shows a large transient in the form of a discontinuity that propagates down a conduit formed by the pre-existing steady state HPS jet. The scales are based on the analysis of the VLBA maps of jets in HPS that are described in the text and the light curves in Figure 2. The details of the time evolution are described in the text. Note that there are no VLBA images of this transient stage and it is a speculative model.

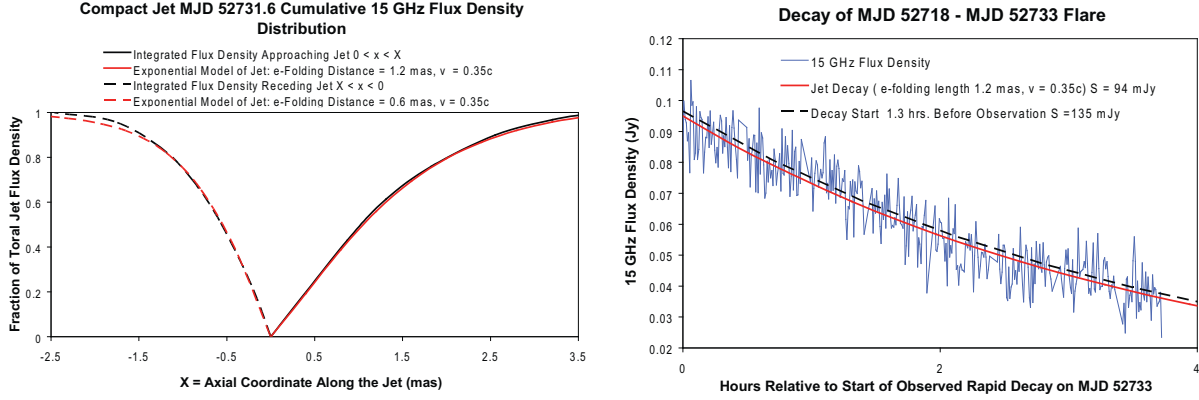


Fig. 4.— The solid (dashed) black curve in the left frame is the cumulative 15 GHz flux density along the approaching (receding) jet on MJD 52731.6. The red solid (dashed) curve in the left hand frame is the output of the exponentially decaying linear source model (described in Section 2.3) of the effective emissivity (i.e., the resultant emissivity arising from the intrinsic emissivity, synchrotron self absorption and Doppler beaming) of the approaching (receding) jet after blurring by the finite beam width of VLBA and interstellar scintillation. The intrinsic velocity of both jets is  $0.35c$ . The apparent approaching (receding) velocity is  $0.36c$  ( $-0.25c$ ). The right hand frame shows the 15 GHz flux density as a function of time for the decay of the steady state HPS jet displayed on the left hand side, that was imaged 1.6 days earlier. The model of the decay is a plot of Equation (13) that is based on the scenario in Figure 3. The modeled jet decay is overlaid on the observed HPS decay from the top frame of Figure 2. Note that there are two fits to the data. One assumes the decay start was synchronous with the observation start time (the solid red curve). The other assumes the decay started 1.3 hours earlier (the black dashed curve).

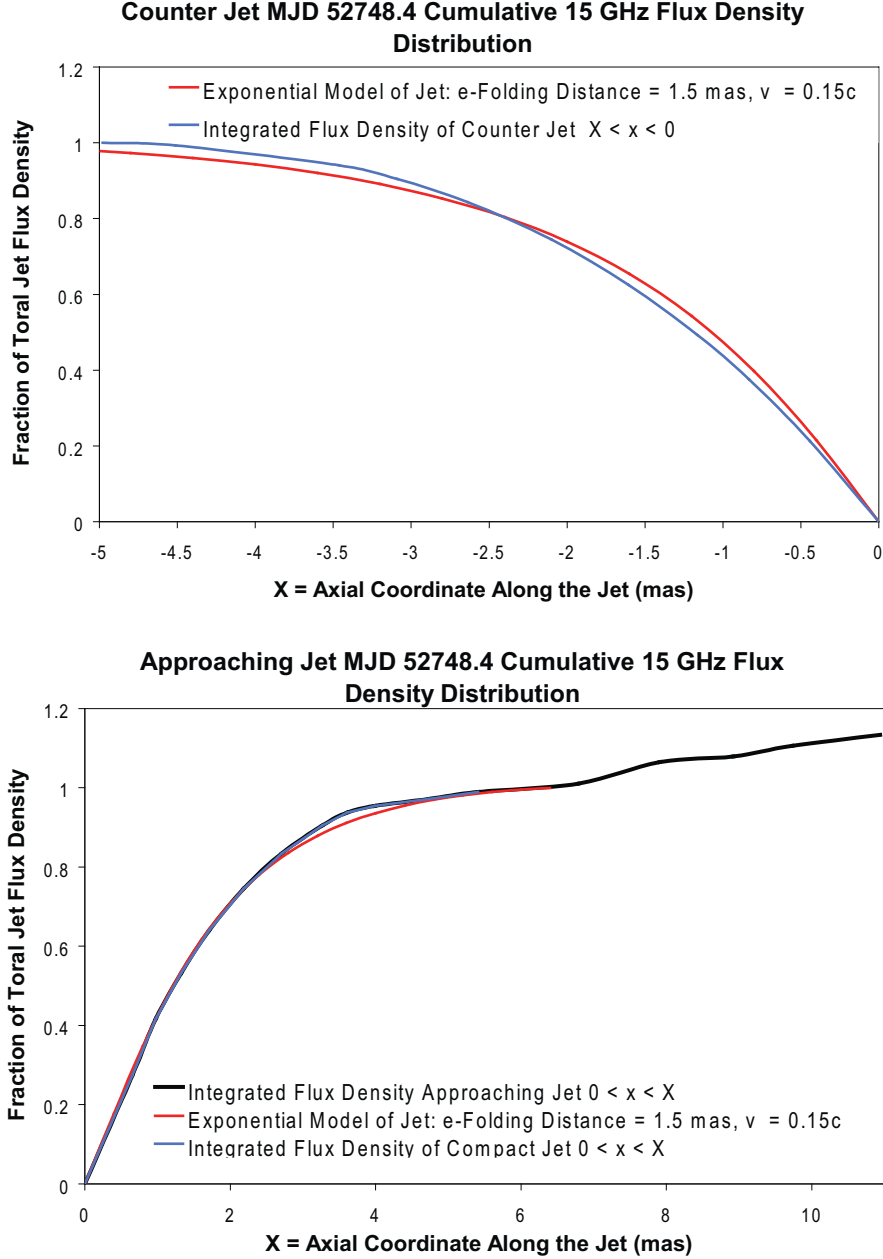


Fig. 5.— The top frame is the fit of the empirical source of effective emissivity of the counter jet on MJD 52748.4. The fit is obtained simultaneously with the fit to the approaching jet in the bottom frame. The comparison of the source to the VLBA image is achieved through the application of Equations (4) - (10). The blue curve represents the cumulative flux density of the compact jet in the radio images. The red curve is the output of the exponentially decaying linear source model of the jet effective emissivity after blurring by the finite beam width of VLBA and interstellar scintillation. The solid black line is the cumulative 15 GHz flux density along the approaching jet on MJD 52748.4. Note the faint discrete ejection 2-4 mas beyond the end of the compact jet. This jet is significantly more symmetric than the jet in Figure 4 (especially if one segregates the discrete emission on the approaching jet side). Consequently, the jet is consistent with a slow intrinsic velocity of  $0.15c$ .

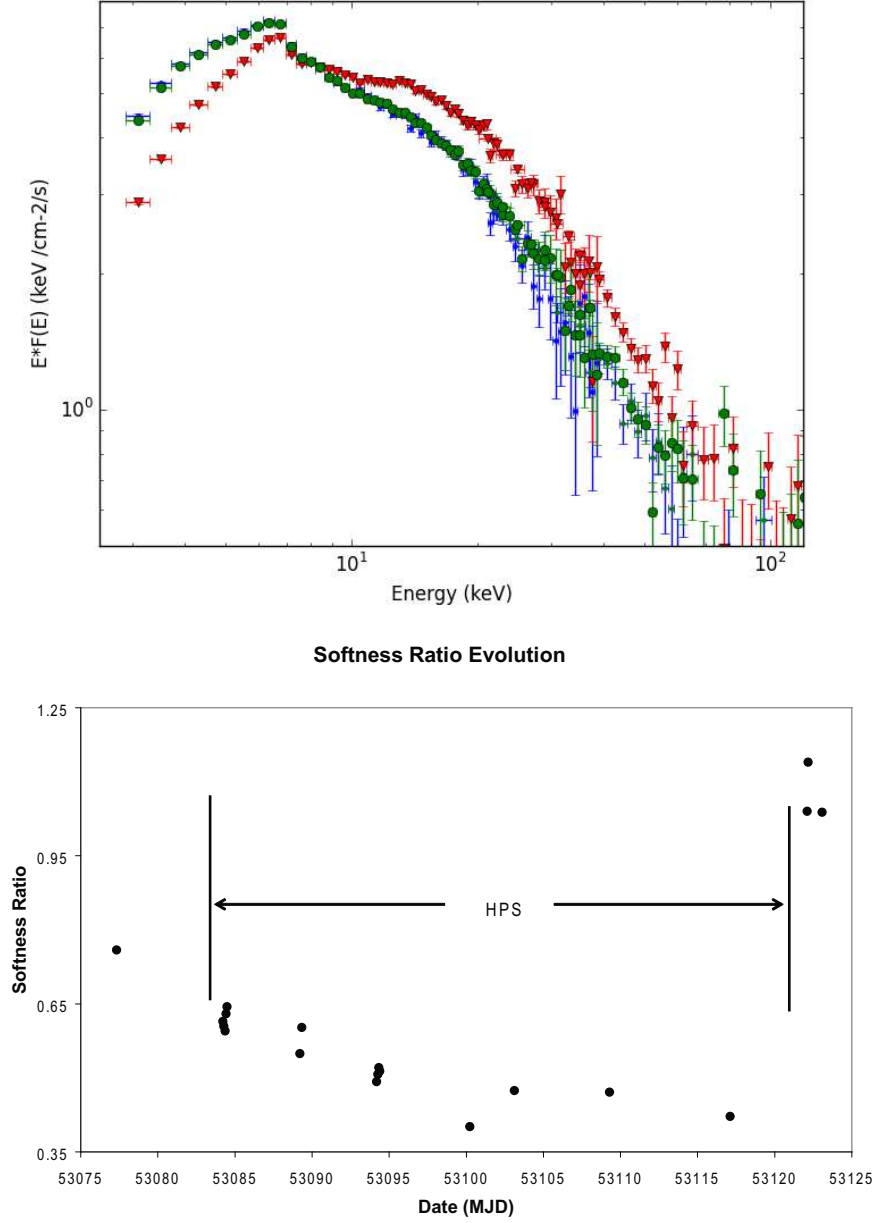


Fig. 6.— The top frame shows the X-ray SEDs during an HPS and during the decay. The red plot is from MJD 53117.114, green from MJD 53122.107 and blue from MJD 53122.179. The SED is much softer during the decay of the HPS state than during the HPS. The bottom frame shows the time evolution of the softness ratio,  $R$ , during the HPS and the decay of the HPS:  $R = F_{1.5-3}/F_{12-50}$ , where  $F_{1.5-3}$  is the intrinsic flux in the interval 1.5 keV - 3 keV and  $F_{12-50}$  is the flux in the interval 12 keV - 50 keV.

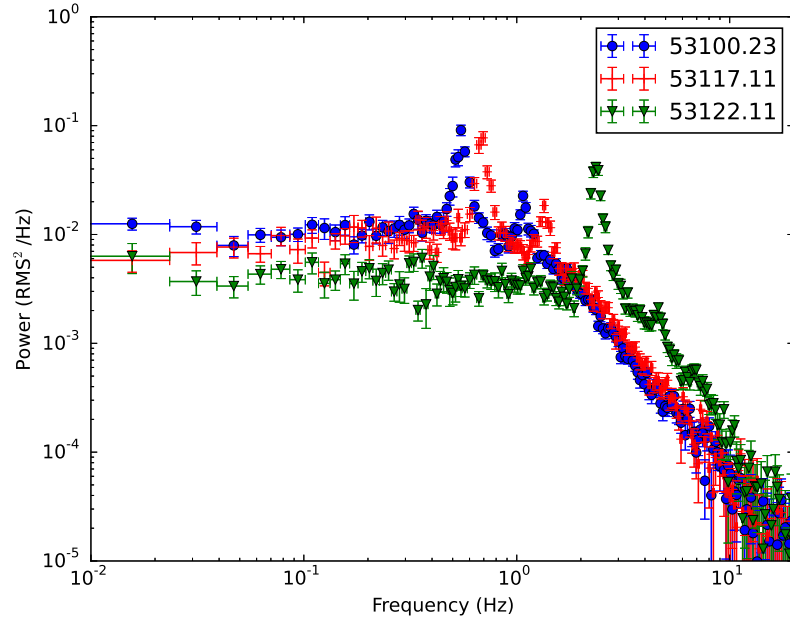


Fig. 7.— The Figure compares the PSD during the HPS. Both the PSD on MJD 53100.230 in blue on MJD 53117.114 in red are from the HPS. The PSD of the combined data from MJD 53122.107 and MJD 53122.179 is plotted in in black.

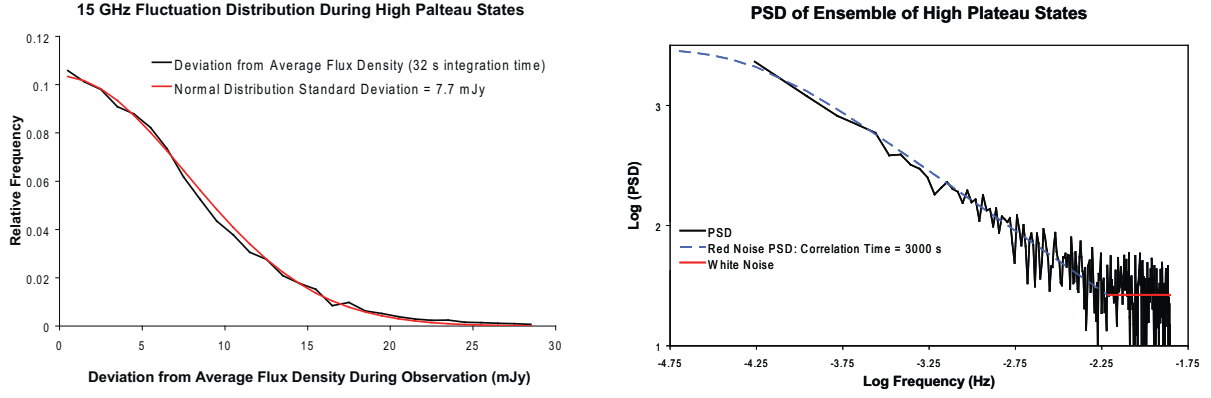


Fig. 8.— The solid red line in the left hand frame is the Gaussian fit to the amplitude spectrum of fluctuations from the ensemble of HPS plotted in black. The right hand frame is the power spectrum of the ensemble of fluctuations. A theoretical red noise power spectrum (with a break to white noise at high frequency) that fits the data closely is plotted as a blue dashed line (solid red line). The correlation time for the red noise in the fit that is displayed is 3000 sec. The fit improves slightly at low frequencies for longer correlation times, but the data sampling is insufficient to constrain the red part of the spectrum.